

Multiple outflows in the planetary nebula NGC 6058

P. F. Guillén^{1*}, R. Vázquez¹, L. F. Miranda^{2,3}, S. Zavala^{4,5}, M. E. Contreras¹,
S. Ayala⁶ and A. Ortiz-Ambriz⁷

¹*Instituto de Astronomía, Universidad Nacional Autónoma de México, Apdo. Postal 877, 22800 Ensenada, B. C., Mexico*

²*Departamento de Física Aplicada, Universidad de Vigo, Campus Lagoas-Marcosende s/n, E-36310 Vigo, Spain*

³*Consejo Superior de Investigaciones Científicas, Serrano 117, E-28006 Madrid, Spain*

⁴*Instituto Tecnológico de Ensenada, Blvd. Tecnológico No. 150, 22780 Ensenada, B. C., Mexico*

⁵*Instituto de Estudios Avanzados de Baja California, A. C., Av. Obregón 1755, 22800 Ensenada, B. C., Mexico*

⁶*Facultad de Ciencias Físico-Matemáticas, Universidad Autónoma de Nuevo León, Av. Universidad s/n., 66451 San Nicolás de los Garza, N. L., Mexico*

⁷*Photonics and Mathematical Optics Group, Tecnológico de Monterrey, Av. Eugenio Garza Sada. 2501, 64849, Monterrey, N. L., Mexico.*

Accepted 2013 April 10

ABSTRACT

We present narrow-band [O III] λ 5007 and H α images, as well as long-slit high-resolution echelle spectra of the planetary nebula NGC 6058. Our data reveal that NGC 6058 is a multipolar planetary nebula of about $\simeq 45$ arcsec in extent and formed by four bipolar outflows that are oriented at different position angles. Assuming homologous expansion for all the structures, and a distance of 3.5 kpc, we obtain polar velocities around $\simeq 68$ km s⁻¹ for three of them. The estimated kinematical ages suggest that the three oldest outflows have been ejected in intervals of ~ 1100 and ~ 400 yr during which, the ejection axis has changes its orientation by $\sim 60^\circ$ and $\sim 40^\circ$, respectively. Although a inner ring-like structure is suggested by the direct images, its kinematics shows that no equatorial ring or toroid exists in the nebula. At the contrary, the long-slit spectra reveal that the ring-like structure corresponds to a fourth outflow that is oriented almost perpendicular to the other three. This fourth outflow is the youngest one and appears to be interacting with the other three, creating a protruding zone that sweeps material in a region almost perpendicular to the major axes of the oldest outflows. This structure also presents two bright arcuate regions along the same direction of the older outflows, and at opposite sides from the central star. From our model, we suggest that NGC 6058 could be an intermediate evolutionary stage between starfish planetary nebulae and multipolar planetary nebula with apparent equatorial lobes.

Key words: ISM: jets and outflows – ISM: kinematics and dynamics – planetary nebulae: individual: NGC 6058

1 INTRODUCTION

A Planetary Nebula (PN) is a physical system composed by a gaseous shell surrounding an evolved star. The shell is a product of the evolution of the star which is often referred as ‘nucleus’ or ‘central star of the PN’. This system corresponds to a particular stage in the evolution of low- to medium-mass stars ($M \leq 8 M_\odot$), between the Asymptotic Giant Branch (AGB) and the white dwarf phases. The interacting stellar wind model (Kwok, Purton & Fitzgerald 1978) and its generalization (Balick 1987; Icke et al. 1989) account for the simplest PN morphologies, namely, spherical, elliptical, and bipolar. However, it is well known that PNe show more complex morphologies, including, e.g., jets, multiple outflows, and point-symmetric structures (see, Acker et al. 1992; Schwarz, Corradi & Melnick 1992; Manchado et al. 1996a).

In some cases, extremely complex morphologies have been found in images obtained with the Hubble Space Telescope¹. Thus, in the last decades, a renewed interest has risen to explain these complex morphologies.

Among these complex morphologies, Manchado, Stanghellini & Guerrero (1996b) defined a new morphological class of PNe they called ‘quadrupolar’, based on the presence of two systems of bipolar lobes in the same PN, which present different orientations but share the same center. Examples of quadrupolar PNe include K 3-24, M 1-75, M 2-46, M 3-28, and M 4-14 (Manchado, Stanghellini & Guerrero 1996b); NGC 6881 (Guerrero & Manchado 1998; Kwok & Su 2005), PNG126.6+01.3 (Mampaso et al. 2006), Kn 26 (Guerrero et al.

* E-mail:fguillen@astro.unam.mx

¹ Many examples of PNe and other objects can be seen at <http://heritage.stsci.edu/gallery/gallery.html> and related sites.

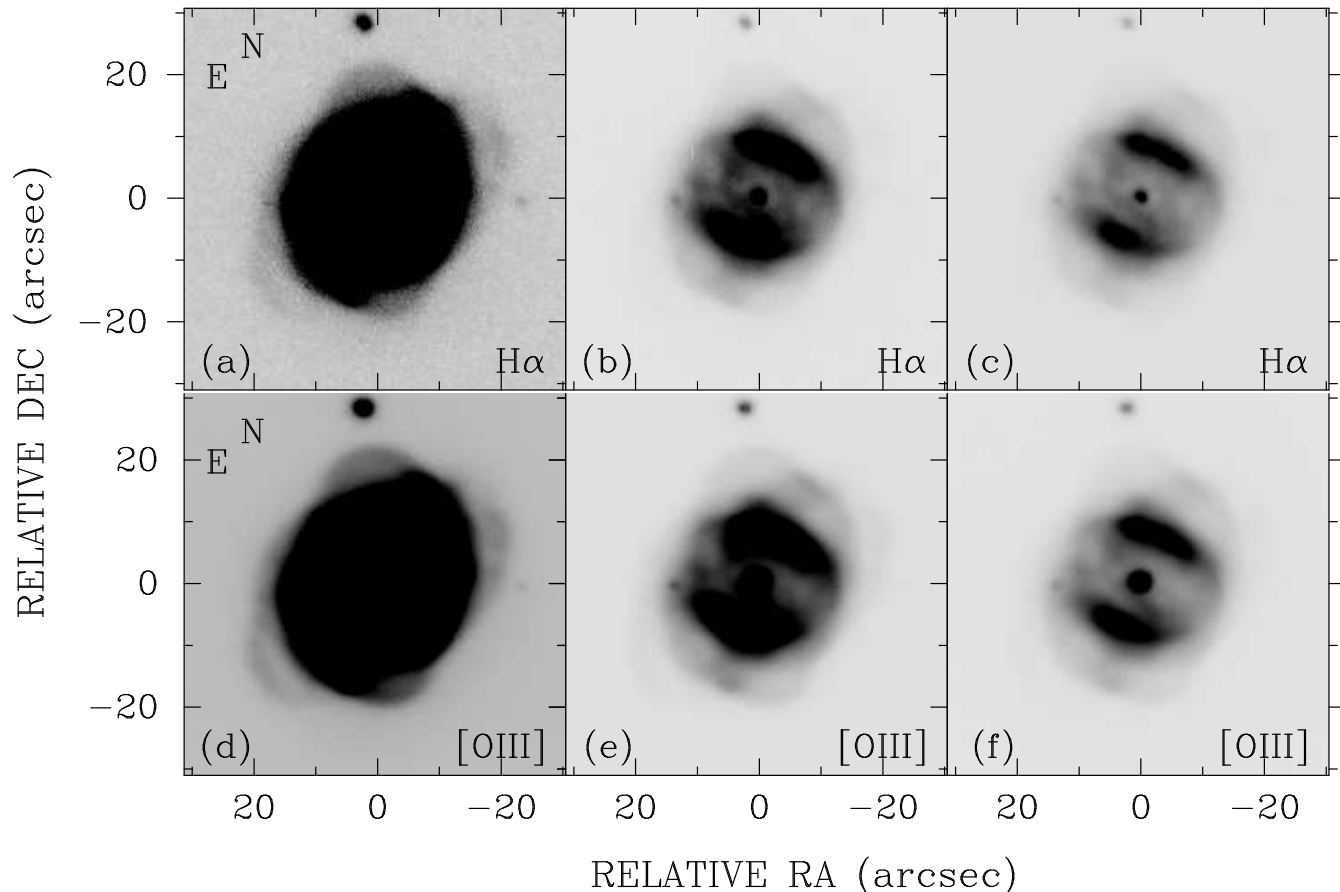


Figure 1. Greyscale displays of NGC 6058. Upper (lower) panels show $H\alpha$ ([O III]) images with arbitrary contrast chosen to enhance the different features present in the nebula.

2013), and NGC 6309 (Vázquez et al. 2008). More extreme is the case of PNe that show more than two bipolar outflows, the so called multipolar or polypolar PNe (e.g. NGC 2440 López et al. 1998, Vázquez et al. 1999; He 2-113, Sahai, Nyman, & Wotten 2000; J320 Harman et al. 2004; NGC 5189, Sabin et al. 2012). Different explanations have been used in literature to explain the presence of more than one system of bipolar lobes, as, for instance, multiple ejections from a binary star (e.g. Velázquez et al. 2012), and bipolar ejections collimated by a warped irradiated disk (e.g. Rijkhorst, Mellema, & Icke 2005). In order to impose constraints on the models for the formation of complex PNe, the analysis of their spatio-kinematical structure has proven to be crucial (e.g. Balick et al. 1987; Miranda & Solf 1992; Corradi & Schwarz 1993; López et al. 1998; Miranda et al. 2006; Guerrero et al. 2008; Vázquez et al. 2008; Vaytet et al. 2009; García-Díaz et al. 2009; Contreras et al. 2010). In particular, high-resolution, long-slit spectra combined with narrow-band images is a powerful technique to obtain the 3D structure of PNe.

In this work, we analyze the morphokinematical structure of NGC 6058 (PN G064.6+48.2), located at $RA(2000) = 16^{\text{h}}04^{\text{m}}26^{\text{s}}.5$, $Dec. (2000) = +40^{\circ}40'56''$, which is a relatively small PN with an apparent elliptical morphology (Manchado, Stanghellini & Guerrero 1996b), but also classified as a multiple-shell PN by Chu et al. (1987). Based on a kinematical study, Sabbadin (1984) concluded that NGC 6058 is an evolved PN in the optically thin phase. He reports expansion velocities of 26 km s^{-1} in [O III] and 23 km s^{-1} in $H\alpha$.

NGC 6058 is a high-excitation PN (Gurzadyan & Egikyan 1991) with relatively low electron densities ($N_e[\text{O II}] \simeq 1400 \text{ cm}^{-3}$, and $N_e[\text{Ar IV}] \simeq 912 \text{ cm}^{-3}$, Wang et al. 2004) and electron temperature $T_e \simeq 13,200 \pm 500 \text{ K}$ (Kaler 1985). Although NGC 6058 appears in a relatively large number of articles (see references in SIMBAD), there is not a detailed analysis of its internal kinematics and morphology that allows us to deduce its 3D structure and the physical processes involved on its formation.

In this paper we present a morphokinematical study of NGC 6058, based on deep imaging and high-resolution, long-slit spectroscopy. Our study reveals that NGC 6058 belongs to the group of multipolar PNe mentioned above. In Section 2 we present our observations and results which are discussed in Section 3.

2 OBSERVATIONS AND RESULTS

2.1 CCD direct images

Direct narrow-band images of NGC 6058 were obtained on 2007 April 18 with the 1.5-m Harold Johnson telescope at the San Pedro Mártir Observatory (OAN-SPM²). The detector was a

² The Observatorio Astronómico Nacional (OAN-SPM) is located at the Sierra de San Pedro Mártir, Baja California, and is operated by the Instituto de Astronomía of the Universidad Nacional Autónoma de México (UNAM).

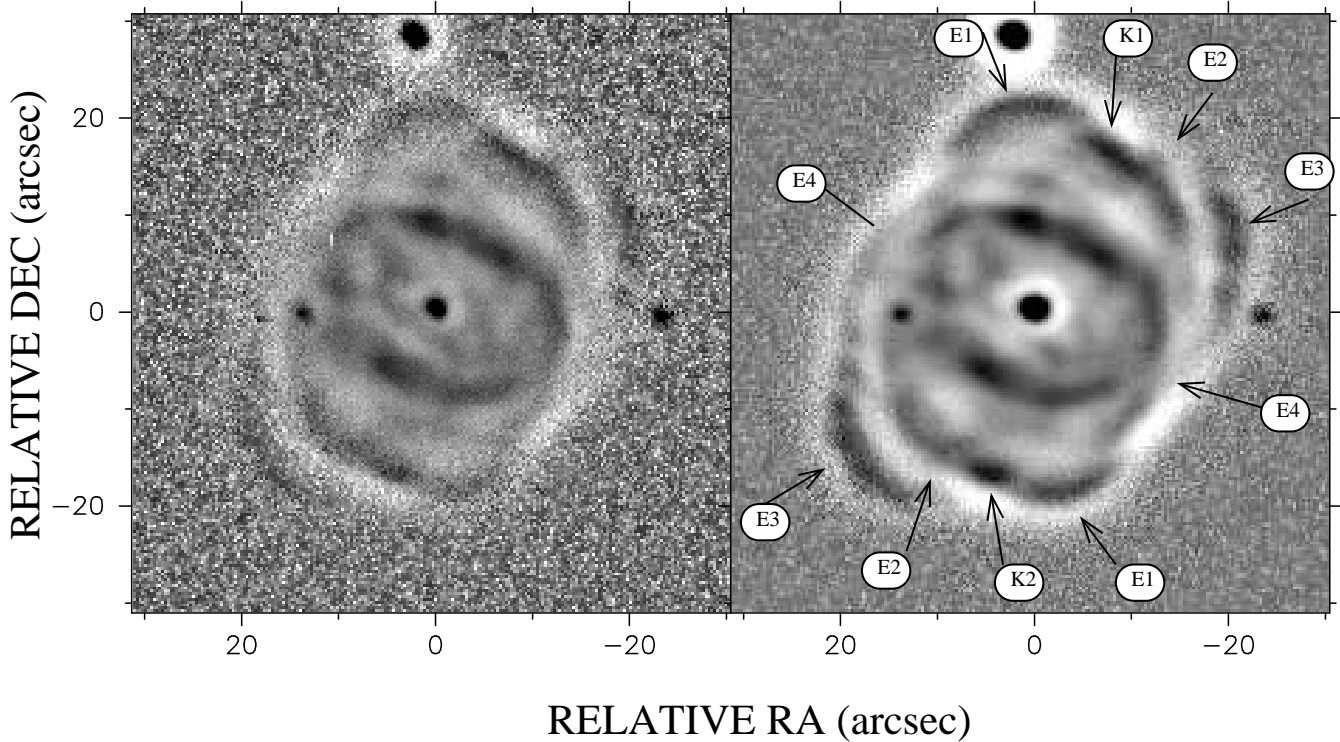


Figure 2. Greyscale $H\alpha$ (left) and $[O\ III]$ (right) images of NGC 6058 after being processed with an unsharp-masking filter. High spatial frequencies are remarked with this technique. The pairs of arcs mentioned in the text are labelled as E1, E2, E3, and E4.

2048 \times 2048 Marconi CCD ($13.5\ \mu\text{m}$ pixel size) with a plate scale of $0.14\ \text{arcsec}\ \text{pix}^{-1}$. The detector was set to binning 2×2 , resulting in a plate scale of $0.28\ \text{arcsec}\ \text{pix}^{-1}$ and a field of view of $4'.8\times 4'.8$. $H\alpha$ ($\lambda_c = 6563\ \text{\AA}$, $\text{FWHM} = 10\ \text{\AA}$) and $[O\ III]$ ($\lambda_c = 5007\ \text{\AA}$, $\text{FWHM} = 50\ \text{\AA}$) filters were employed to acquire the images. Seeing was around $2\ \text{arcsec}$ during observations. Total exposure times were $2100\ \text{s}$ and $3600\ \text{s}$ for the $H\alpha$ and $[O\ III]$ images, respectively. Images were processed using standard techniques of IRAF and they are shown in Fig. 1.

In the $H\alpha$ and $[O\ III]$ images, the nebula resembles an ellipse ($42\times 48\ \text{arcsec}^2$), and recalls the structure previously reported by Chu et al. (1987) (internal shell), characterized by faint polar regions and a bright elliptical ring-like region. However, a detailed inspection of the images (Figure 1) reveals the existence of two point-symmetric pairs of faint arcs-like filaments beyond the brighter emission (panels a and d), which have not been reported before.

In order to enhance these structures, we have obtained unsharp-masking images in $H\alpha$ and $[O\ III]$ that are shown in Fig. 2. These images reveal three pairs of point-symmetric arc-like filaments, labelled E1, E2, and E3, and the ring-like region, labelled E4. The pairs E1 and E3 correspond to the new point-symmetric arcs detected in the $H\alpha$ and $[O\ III]$ images, while E2 seems to trace the polar caps of the elliptical shell found by Chu et al. (1987). Thus, E1, E2, and E3 seem to be the polar caps of ellipses whose semi-major axes have different positions angles. The pair E1 is oriented at $\text{PA} \simeq 7^\circ$ and presents an extent of $\simeq 38\ \text{arcsec}$. E2 is oriented at $\text{PA} \simeq -32^\circ$ and its extent is $\simeq 33\ \text{arcsec}$. Between E1 and E2 two enhanced emission regions (denoted K1 and K2, Fig. 2) can be distinguished at opposite sides of the central star. The pair E3 is oriented at $\text{PA} \simeq -52^\circ$ and presents an extent of $\simeq 44\ \text{arcsec}$. The

ring-like structure E4 presents a size of $\simeq 16\ \text{arcsec}\times 27\ \text{arcsec}$, with the major axis oriented at $\text{PA} \simeq 65^\circ$. Contrary to the other pairs, the polar caps of E4 are only marginally detected, whereas the regions around its minor axis are the brightest ones of the nebula.

The images strongly suggest that NGC 6058 is a multipolar PN containing three bipolar outflows at different orientations and an equatorial ring-like structure that is tilted with respect to the line of sight. In some respects, the new images of NGC 6058 show a structure that is reminiscent of starfish PNe (Sahai 2000), that present multipolar lobes accompanied by an equatorial ring-like structure. However, as we will see below, the kinematics of NGC 6058 shows that important projection effects are involved in this PN and that E4, rather than an equatorial ring, corresponds to a limb-brightening barrel-like shell, similar to that seen in the $H\alpha$ image of NGC 7354 (Contreras et al. 2010).

We have also obtained an $[O\ III]/H\alpha$ image ratio that is presented in Fig. 3. This image shows enhancements of the $[O\ III]$ emission at the arcs E1, E2, and E3. According to Medina et al. (2009), the $[O\ III]$ enhancement indicates the presence of shocks at the locations of the arcs, which suggests that E1, E2, and E3 are related to collimated outflows.

2.2 Long-slit echelle spectroscopy

High-resolution, long-slit spectra were obtained on 2003 June 6 with the Manchester Echelle Spectrograph (MES; Meaburn et al. 2003) in the 2.1-m telescope at OAN-SPM. A Site $24\text{-}\mu\text{m}\ \text{pix}^{-1}$ CCD with 1024×1024 pixels was used as detector in 2×2 binning mode ($0.6\ \text{arcsec}\ \text{pix}^{-1}$ plate scale). The spectra were centered at the $H\alpha$ emission line using a filter ($\Delta\lambda=90\ \text{\AA}$) to isolate the 87^{th} or-

der (0.1 \AA pix^{-1} spectral scale). Exposure time was 900 s for each spectrum.

A second set of spectra were obtained on 2007 July 17 and 18 using the same telescope, instrument and detector described above. In this case, the spectra were centered at the $[\text{O III}]\lambda 5007$ emission line using a filter ($\Delta\lambda=50\text{\AA}$) to isolate the 114th order ($0.08 \text{ \AA pix}^{-1}$ spectral scale). In this case, exposure time was 1800 s for each spectrum.

Data were calibrated using standard techniques for long-slit spectroscopy of IRAF. The slit width was $150 \mu\text{m}$ (1.9 arcsec). The resulting spectral resolution (FWHM) is $\simeq 12 \text{ km s}^{-1}$ (accuracy $\pm 1 \text{ km s}^{-1}$), as measured from the lines of the ThAr calibration lamp. Seeing was around 1.5 arcsec during the observations.

Figure 4 shows the slit positions used to acquire the spectra, superimposed on the $[\text{O III}]$ unsharp-masking image and labeled as follows: S1 (PA = 7°), S2 (PA = -23°), S3 (PA = -55°), and S4 (PA = 72°), for the spectra taken in $[\text{O III}]$ (all of them crossing the central star), and S5, S6, and S7 for the spectra taken in $\text{H}\alpha$, all of them oriented at PA = 90° with S6 crossing the central star and S5 and S7 shifted 7 arcsec towards the North and the South, respectively. The corresponding Position-Velocity (PV) maps are shown in Figures 5 and 6 for $[\text{O III}]$ and $\text{H}\alpha$, respectively. In Figure 5, rows in the PV maps array correspond to the slit positions S1, S2, S3, and S4. Columns 1 to 3 show the same spectrum with different contrast levels. Velocity axes of all the PV maps are relative to the systemic velocity whereas spatial axes are relative to the location of the central star, or its Right Ascension, in the cases of S5 and S7. The systemic velocity was obtained from the velocity splitting of the spectral lines observed at the position of the central star. We obtain $V_{\text{LSR}} \simeq 23 \pm 1 \text{ km s}^{-1}$ ($V_{\text{Hel}} \simeq 6 \pm 1 \text{ km s}^{-1}$), in good agreement with the value of $\simeq 20 \pm 3.3 \text{ km s}^{-1}$ reported by Schneider et al. (1983). In addition, the mean value of the expansion velocity, measured at the position of the central star, is $v_{\text{ex}} = 37 \text{ km s}^{-1}$.

On the PV maps (Figure 5), the arc-like structures E1, E2, and E3 identified in the images (Fig. 2; right) have a corresponding structure in the spectra. Each pair appear as the tips of an apparent velocity ellipse. In the case of E1, emission can be identified at S1 with an extent of $\pm 19 \text{ arcsec}$ from the central star. The radial velocities at the tips of E1 differ by 7.6 km s^{-1} , with the northern region being redshifted and the southern region blueshifted. E2 can be identified at S2 and S3 at $\pm 16.4 \text{ arcsec}$ from the central star. The northwestern tip of E2 is blueshifted by 4.2 km s^{-1} while the southeastern tip is redshifted by the same amount. We note the existence of two bright knots on the PV map separated by $\simeq 33 \text{ arcsec}$ and at the systemic velocity, which correspond to the knots K1 and K2 (see Fig. 2). Finally, E3 is identified at S3 as two extended features with a spatial extent of $\pm 23 \text{ arcsec}$ and a difference of radial velocities of 36 km s^{-1} . The northwestern region of E3 redshifted whereas its southeastern region is blueshifted.

The PV maps at S1, S2, and S3 also show bright ‘‘knots’’ located close to the systemic velocity. These bright ‘‘knots’’ corresponds to the bright arcs of the ellipse identified in the image as E4. Remarkably, the radial velocity of these features is very similar to the systemic velocity. This indicates that the bright arcs should move mainly in the plane of the sky and, therefore, it rules out that E4 corresponds to a tilted ring-like structure. Moreover, the bright ‘‘knots’’ appear on the PV maps as a part of a velocity ellipse, indicating that they belong to a three dimensional structure. The velocity ellipse is well defined at S1 and S2 but presents strong distortions at S3 and S4. In particular at S4, the velocity ellipse seems to be open and its apparent polar regions present a complex

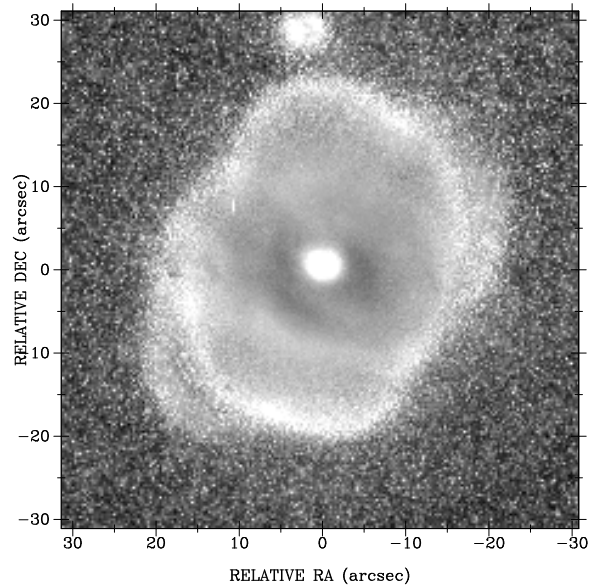


Figure 3. Greyscale image of the $[\text{O III}]/\text{H}\alpha$ ratio of NGC 6058. High and low values of this ratio are in white and dark gray, respectively.

kinematics. These regions correspond to the polar regions of E4 in the images, which are noticeably fainter than the arcs.

Thus, the PV maps reveal the existence of a distorted probably ellipsoidal structure that can be only identified in the PV maps but not in the images. This structure, which we continue labeling E4, is tilted in such a way that its NE part is blueshifted and its SW part is redshifted. Maximum radial velocities of $\simeq \pm 53 \text{ km s}^{-1}$ are observed at S4 where a maximum angular size of 24 arcsec is also observed. This implies that the major axis of E4 should be oriented close to PA 72° , where the maximum distortions are also observed. This orientation is almost perpendicular to that of the point-symmetric arcs E1, E2, E3.

The $\text{H}\alpha$ emission feature at S6 (Fig. 6) shows a structure very similar to that observed in $[\text{O III}]$ at S4 (Fig. 5). In particular, a tilted velocity ellipse is observed with the eastern region blueshifted and the western region redshifted. In addition, a marginal evidence of the expansion of the East and West sides of E2 is observed in S5 and S7 slit positions, respectively ($V_{\text{exp}} \simeq 30 \text{ km s}^{-1}$).

A final note about the spectra around $\text{H}\alpha$ is that the high-excitation nature of NGC 6058 results evident in them, given that there is not any detection of $[\text{N II}]\lambda 6548, 6583$ emission lines in these spectra. On the contrary, the high-excitation $\text{He II}\lambda 6560$ emission line is marginally detected in the spectra, with an intensity of $\leq 3\%$ that of $\text{H}\alpha$. This implies that the contribution of $\text{He II}\lambda 6560$ to the $\text{H}\alpha$ image (Fig. 1) can be considered negligible.

3 DISCUSSION

From the morphological and kinematical data mentioned in the last section, we have identified three bipolar outflows (E1, E2, and E3) whose small differences between the radial velocities of their polar caps suggest that these outflows were ejected almost in the plane of the sky. A fourth structure (E4), that easily can be misidentified as an equatorial ring in the images, is clearly recognized as an ellipsoidal-like shell in the PV maps. The corresponding features of this ellipsoid in the PV maps show a higher difference in its

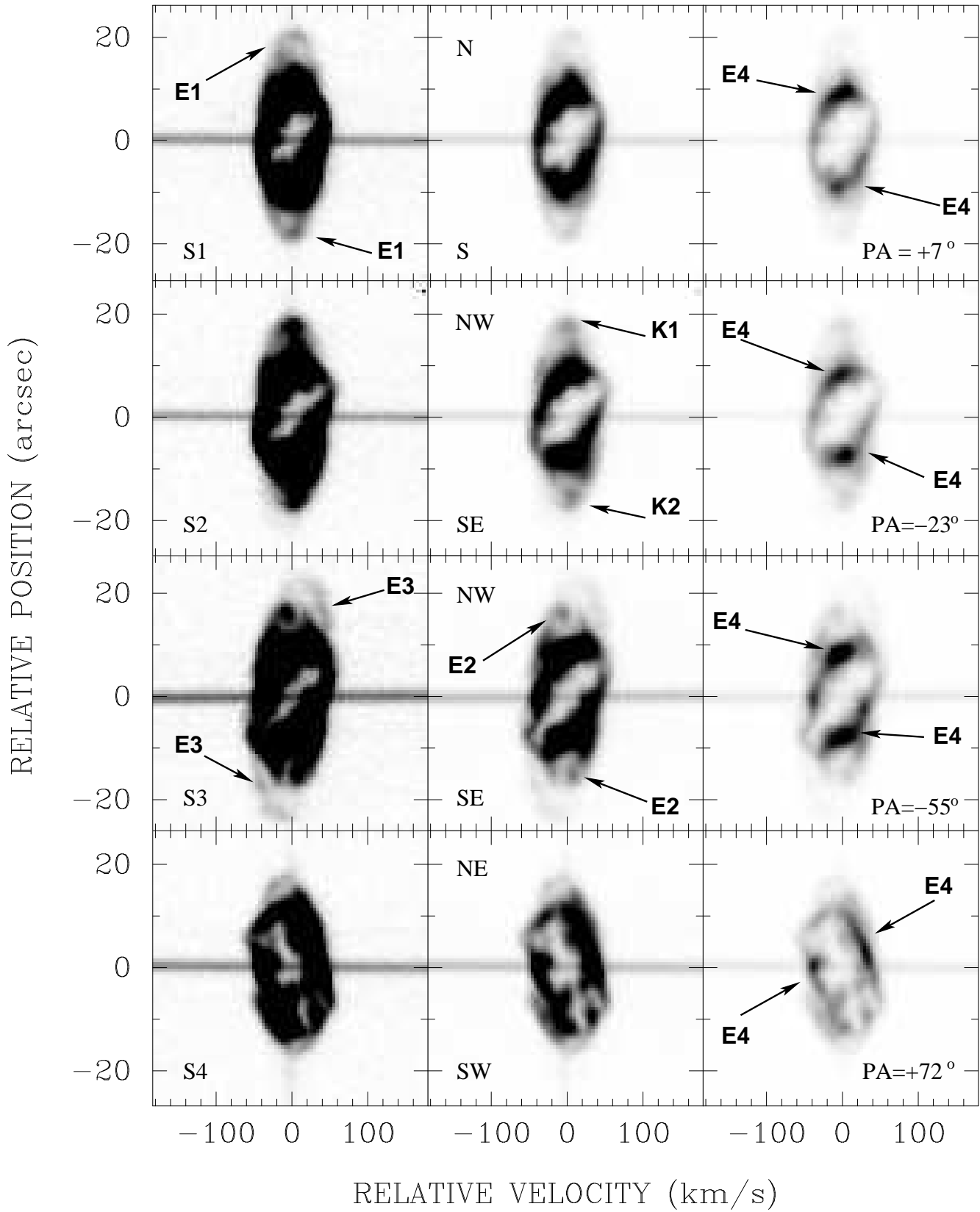


Figure 5. Position-Velocity (PV) maps of the [O III]λ5007 emission line corresponding to the S1, S2, S3, and S4 slit positions (rows). Three different grey levels (columns) were arbitrary chosen in order to highlight different features in the maps. Kinematical features corresponding to E1, E2, E3, and E4 are labelled in the figure.

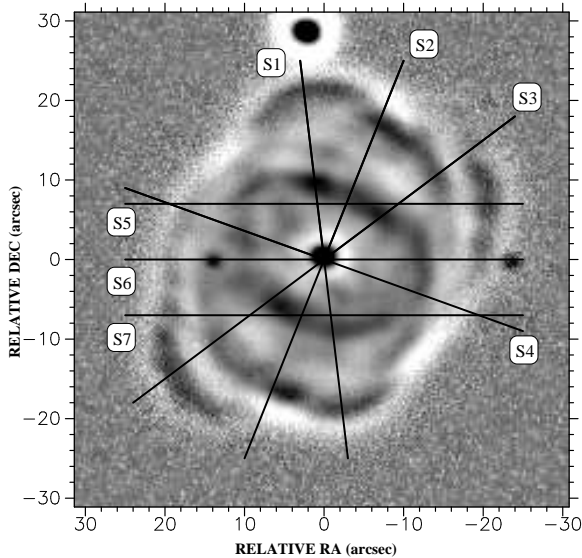


Figure 4. Unsharp-masked image of NGC 6058 in [O III]. Lines indicate the different slit positions that were used to obtain our high-dispersion spectra. Slits labeled as S1, S2, S3, and S4, correspond to the spectra centered on [O III] λ 5007, whereas slits labeled as S5, S6, and S7, correspond to the spectra centered on H α .

maximum radial velocities, suggesting that its orientation is very different with respect the outflows E1, E2, and E3.

Based on the apparent elliptical shape of the outflows in both, images and PV maps, we have modeled the structures E1, E2, E3, and E4 as ellipsoids. As expected for these structures, we have assumed that each ellipsoid projects an ellipse in the plane of the sky which is fitted using IRAF+DS9 software. The ellipses were obtained trying to get the best size and shape fits for the polar caps E1, E2, and E3, and for the bright arcs of E4. Figure 7 shows the fits for the case of the direct image. Using these ellipses as the projection in 3D of the ellipsoids, we fit other parameters (inclination angle, velocity field, etc.) in order to reproduce the PV maps.

For each ellipsoid, the apparent polar radius and velocity are measured from the image and the corresponding long-slit spectrum, whereas the equatorial radius and velocity are obtained from the fitted ellipse and the kinematical model, respectively. For the model we have always assumed a homologous expansion velocity ($v \propto r$) and small deviations ($\lesssim 20^\circ$) around 90° for the inclination angle (i). A sketch showing the main parameters of an ellipsoidal shell (a), as well as the observer view for the image (b) and the PV map (c), are presented in Figure 8. With the considerations mentioned above, and following the nomenclature in Figure 8(a), it can be demonstrated that

$$\tan \alpha = \left(\frac{r_e}{r_{pz}} \right) \left(\frac{v_{px}}{v_e} \right)$$

where r_e is the equatorial radius (semi-minor axis); r_{pz} is the apparent polar radius (projected semi-major axis); v_e is the equatorial velocity, and v_{px} is the apparent polar velocity (radial component). The inclination angle of the ellipsoid major axis, with respect to the line-of-sight, i , can be derived as $i = 90^\circ + \alpha$, if the North pole of the ellipsoid is moving away from the observer, and as $i = 90^\circ - \alpha$ if coming closer.

It is important to mention that, as can be noted in Fig 8, the radial velocity measured at the position of the central star, v_{cx} , is

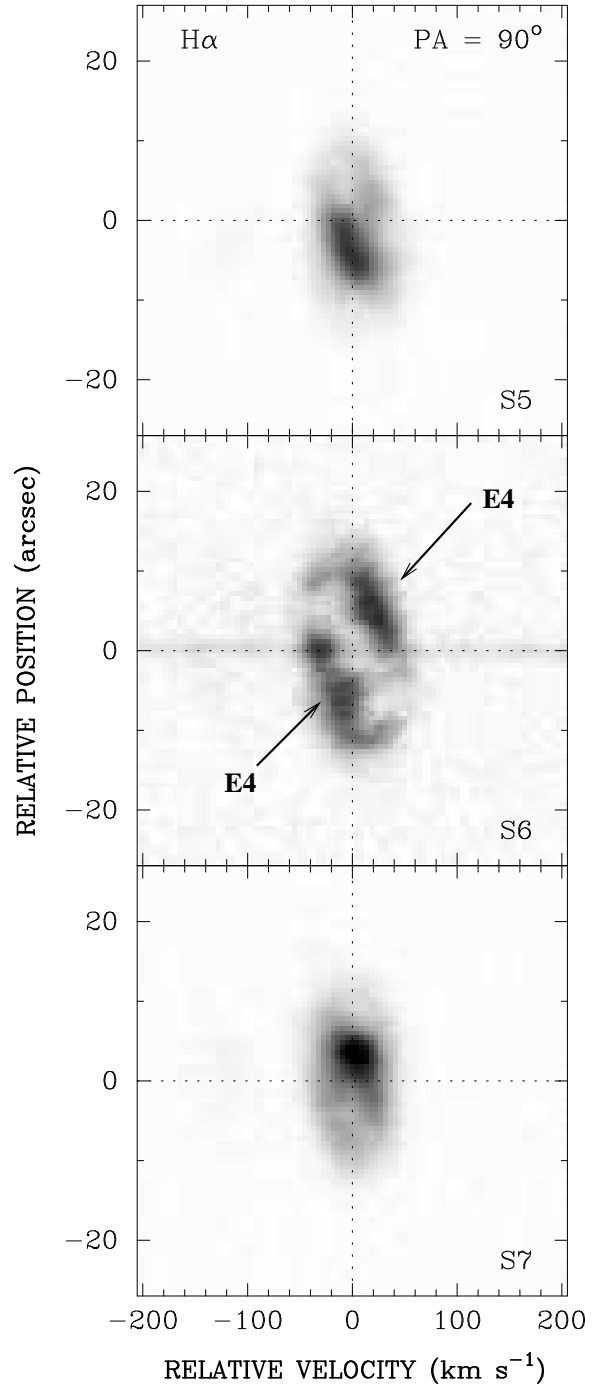


Figure 6. Position-Velocity maps in H α . Labels correspond to slit position shown in Fig. 4. East is up and West is down.

different than v_e as well as v_{ex} . However, using a rough approximation of the polar-to-equatorial ratio $r_p/r_e \approx 2$ (which is reasonable, given the semi-axes ratios of the ellipses), assuming a “small” value for $\alpha \approx 20^\circ$, and using the cartesian equation for a vertical ellipse, we have estimated the ratio

$$\frac{v_{cx}}{v_e} = \frac{r_{cx}}{r_e} = \frac{r_p/r_e}{\sqrt{\sin^2 \alpha + (r_p/r_e)^2 \cos^2 \alpha}} \approx 1.047$$

i.e., an error $\lesssim 5\%$ is committed when considering the approximation $v_e \approx v_{cx}$. Therefore, we will use this approximation and its

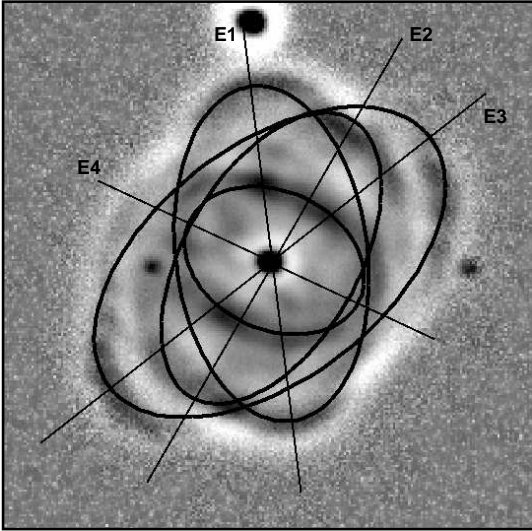


Figure 7. We present the four ellipses model that best fit the morphology observed in NGC 6058. The ellipses are superimposed on the [O III] $\lambda 5007$ unsharp-masking image shown in Fig. 2b.

associated error to estimate α , i , and the other parameters in the following calculations.

Polar radius and velocity can be now obtained using the relationships for the projected r_p and the homologous velocity law, respectively

$$r_p = \frac{r_{pz}}{\sin i}; \quad v_p = v_e \left(\frac{r_p}{r_e} \right) = v_{ex} \left(\frac{r_{pz}}{r_e \sin i} \right).$$

In addition, the kinematical age τ_k can be derived as

$$\left[\frac{\tau_k}{\text{yr}} \right] = 4744 \times \left[\frac{r_p}{\text{arcsec}} \right] \left[\frac{D}{\text{kpc}} \right] \left[\frac{v_p}{\text{km s}^{-1}} \right]^{-1}$$

where D is the distance from the Earth to the nebula (in kpc). Values of i , r_p , v_p , and τ_k , obtained for all the ellipsoids and assuming a distance of 3.5 kpc (Cahn, Kaler & Stanghellini 1992), are presented in Table 1. It is important to mention that E4 was excluded from Table 1, given that it is not possible to obtain a suitable kinematic model for this ellipse. As we will explain below, we interpret this as the result of outflows interaction. However, as a reference only, we propose the following limits for this ratio

$$1.3 \lesssim \frac{r_p}{r_e} \lesssim 2.$$

where the lower limit corresponds to the apparent axes ratio (r_{pz}/r_e) seen in E4, and the upper limit was chosen as a reasonable value given the apparent polar-to-equatorial ratios from the other ellipses. Using these values, the possible inclination angle for such ellipse would be between 50° and 130° . Consequently, a kinematical age for E4 can be estimated as $\tau_k \approx 3400$ yr. However, as we mentioned above, this value must be taken cautiously.

As can be noted in Table 1, given the uncertainties in the kinematical ages, it is not simple to describe the sequence of events that have occurred in the formation of NGC 6058. Nevertheless, based on the kinematical ages as well as on the orientation of the structures, we propose a scenario in which a series of bipolar outflows could shape the morphology of NGC 6058. In our proposal, the first outflow was E3 along PA $\simeq -52^\circ$. The second ejection

was E1 along PA $\simeq 7^\circ$, involving a change in the orientation of the ejection axis of $\simeq 60^\circ$ with respect to that of E1. The third ejection was E2 along PA $\simeq -30^\circ$ that involves a change of orientation of $\simeq 40^\circ$ with respect to E1. We note that E3 and E1 are ejected with their northern/northwestern half pointing away from the observer whereas the northwestern half of E2 points towards the observer.

Moreover, the deduced kinematical ages (Table 1) suggest a time span of ~ 1100 yr between the two first collimated ejections and only ~ 400 yr between the second and the third. These results point to the existence of episodic ejections with changes in the orientation of the main axis, suggesting precession of the collimation axis. About $\gtrsim 1000$ yr after ejection of E2, a new shell is formed which is identified with E4. In this case, the main ejection axis has largely changed with respect to that of E1–E3, as the polar axis of E4 is almost perpendicular to the previous outflows. Our data strongly suggest that E4 interacts with the previous outflows. The bright arc-like regions observed in the direct images are probably a result of the interaction of the equatorial regions of E4 with parts of E1–E3. Furthermore, the large kinematical distortions observed in E4 along PA around 72° suggest that E4 also interacts with the equatorial regions of the previous outflows and protrudes. We note that this interaction may result in a deceleration of E4 and, therefore, the deduced kinematical age of 3400 yr is probably an upper limit, implying that E4 has been formed noticeably later than the previous outflows.

As a result of this study we can conclude that NGC 6058 belongs to the group of multipolar PNe. It is interesting to compare NGC 6058 with other multipolar PNe. In particular, we find remarkable similarities between NGC 6058 and the so called ‘starfish PNe’ (Sahai 2000). These PNe present three or four pairs of bipolar lobes and an bright elliptical ring-like structure that can be interpreted as a tilted equatorial ring. We may relate the E1, E2, and E3 outflows with the multiple pairs of lobes of starfish PNe, and the bright arcs corresponding to E4 with the equatorial ring of the starfish. However, in NGC 6058 our kinematical data reveal that the bright arcs do not trace a tilted equatorial ring but a part of an ellipsoid shell. In this respect, it would be interesting to study the internal kinematical of starfish PNe in order to check whether the observed elliptical rings have the kinematics expected from a tilted ring or, at the contrary, they trace an ellipsoidal shell, as in the case of NGC 6058.

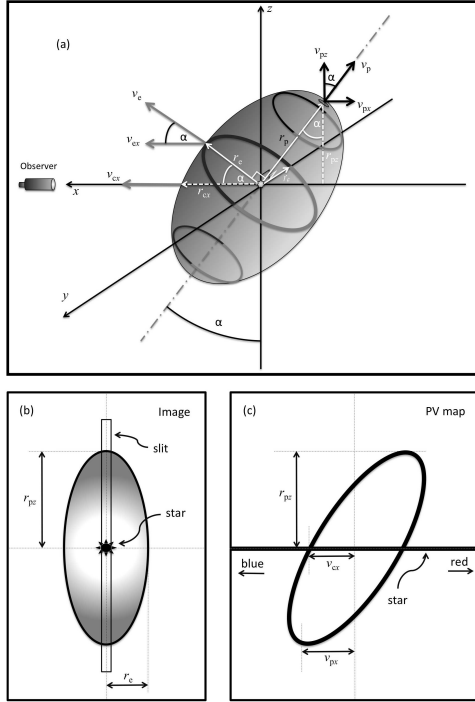
It is interesting to speculate about the possible future evolution of NGC 6058. In particular, the polar regions of E4 could break and expand at a higher velocity, creating, after some time, a pair of large bipolar structures. If so, NGC 6058 would consist in a pair of extended bipolar structures, accompanied of smaller bipolar lobes around its equatorial region, which would correspond to E1–E3. This scenario could provide an explanation for some PNe like Hb 5 and K 3-17 (Miranda, Ramos-Larios & Guerrero 2010; López et al. 2012) in which large bipolar lobes are observed accompanied by secondary smaller lobes around the equator of the largest ones. By all these comments, we suggest that NGC 6058 could be an intermediate evolutionary stage between starfish PNe and PNe with equatorial bipolar lobes.

4 CONCLUSIONS

We have carried out a morphokinematic analysis of the planetary nebula NGC 6058, based on direct imaging and high-dispersion spectroscopy. NGC 6058 can be described as a multipolar PN, formed by three bipolar outflows with different orientations and

Table 1. Parameters of ellipsoids measured and derived from models: position angle (PA), semi-minor axis (r_e), apparent semi-major axis (r_p), equatorial and polar apparent velocities (v_e) and (v_p), inclination angle (i), semi-major axis (r_p), polar velocity (v_p), and kinematical age (τ_k).

	PA ($^\circ$)	r_e (arcsec)	r_{pz} (arcsec)	v_{cx} (km s^{-1})	v_{px} (km s^{-1})	i ($^\circ$)	r_p (arcsec)	v_p (km s^{-1})	τ_k (yr)
E1	+7	11 ± 1	19 ± 1	37 ± 2	3.8 ± 1	93 ± 2	19 ± 1	67 ± 8	4800 ± 600
E2	-30	10 ± 1	18 ± 1	37 ± 2	4.2 ± 1	86 ± 2	18 ± 1	69 ± 9	4400 ± 600
E3	-52	13 ± 1	23 ± 1	37 ± 2	18 ± 1	106 ± 2	24 ± 1	67 ± 10	5900 ± 600

**Figure 8.** (a) A sketch of an expanding ellipsoidal structure, whose semi-major axis has an inclination angle α respect to the plane of the sky, seen from an observer on Earth. Main physical parameters are labeled. (b) The ellipse (image) seen by the observer. (c) The position-velocity map (spectrum) from a slit crossing the major axis.

polar velocities around $\sim 68 \text{ km s}^{-1}$, as well as a distorted ellipsoidal inner shell with its major axis almost perpendicular to those of the other three outflows. Assuming homologous expansion for all the structures and a distance of 3.5 kpc, we obtain kinematical ages ranged from ~ 3400 to ~ 5900 yr for the different outflows. Our data suggest a certain systematic behaviour in the changes of the orientation of the main axis, which points out to episodic, precessing ejections in NGC 6058. The ellipsoidal inner shell is released much after than the three collimated outflows and its kinematics reveals clear signs of interaction with the previous ejections. A comparison with other multipolar PNe suggests that NGC 6058 could be an intermediate stage between (young) starfish PNe and more evolved PNe that show a large pair of bipolar lobes and much smaller equatorial lobes.

ACKNOWLEDGMENTS

We are grateful to the staff of OAN-SPM, specially to Mr. Gustavo Melgoza-Kennedy, our telescope operator, for his assistantship

during observations. This paper has been supported by Mexican grant IN109509 (PAPIIT-DGAPA-UNAM). LFM is partly supported by grant AYA2011-30228-C03.01 of the Spanish Ministerio de Economía y Competitividad (MINECO) and by grant IN845B-2010/061 of Xunta de Galicia (Spain), all of them partially funded by FEDER funds. SZ acknowledges support from the UNAM-ITE collaboration agreement 1500-479-3-V-04. SA acknowledges support from the UNAM-UANL collaboration agreement. This research has made use of the SIMBAD database, operated at CDS, Strasbourg, France. IRAF is distributed by the National Optical Astronomy Observatories, which are operated by the Association of Universities for Research in Astronomy, Inc., under cooperative agreement with the National Science Foundation. We thank our anonymous referee for valuable comments which have improved this article. Authors want to dedicate this paper in memorial of Gaby García-Ruiz, member of the OAN-SPM staff, who passed away.

REFERENCES

- Acker A., Marcout J., Ochsenbein F., Stenholm B., Tylenda R., 1992, Strasbourg ESO Catalogue of Galactic Planetary Nebulae. Part 1; Part 2. European Southern Observatory, Garching
- Balick, B. 1987, AJ, 94, 671
- Balick B., Bignell C. R., Hjellming R. M., Owen R., 1987, AJ, 94, 948
- Cahn J. H., Kaler J. B., Stanghellini L., 1992, A&A, 94, 399
- Chu Y.-H., Jacoby G. H., Arendt R., 1987, ApJSS, 64, 529
- Contreras M. E., Vázquez R., Miranda L. F., Olguín L., Zavala S., Ayala S., 2010, AJ, 139, 1426
- Corradi R. L. M., Schwarz H. E., 1993, A&A, 278, 247
- García-Díaz M. T., Clark D. M., López J. A., Steffen W., Richer M. G., 2009, ApJ, 699, 1633
- Guerrero M. A., Manchado A., 1998, ApJ, 508, 262
- Guerrero M. A., Miranda L. F., Riera A., Velázquez P. F., Olguín L., Vázquez R., Chu Y.-H., Raga A., Benítez G., 2008, ApJ, 683, 272
- Guerrero M. A., Miranda L. F., Ramos-Larios G., Vázquez R., 2013, A&A, 551, A53
- Gurzadyan G. A., Egikyan A. G., 1991, Ap&SS, 181, 73
- Harman D. J., Bryce M., López J. A., Meaburn J., Holloway A. J., 2004, MNRAS, 348, 1047
- Herrero A., Manchado A., Mendez R. H., 1990, Ap&SS, 169, 183
- Rijkhorst E.-J., Mellema G., Icke V., 2005, A&A, 444, 849
- Icke V., Preston H. L., Balick B., 1989, AJ, 97, 462
- Kaler J. B., 1985, ApJ, 290, 531
- Kwok S., Su K. Y. L., 2005, ApJ, 635, L49
- Kwok S., Purton C. R., FitzGerald P. M., 1978, ApJ, 219, L125

- López J. A., Meaburn J., Bryce M., Holloway A. J., 1998, *ApJ*, 493, 803
- López J. A., García-Díaz Ma. T., Steffen W., Riesgo H., Richer M. G., 2012, *ApJ*, 750, 131
- Mampaso A. et al., 2006, *A&A*, 458, 203
- Manchado A., Guerrero M. A., Stanghellini L., Serra-Ricart M., 1996a, *The IAC Morphological Catalog of Northern Galactic Planetary Nebulae*. IAC, La Laguna, Spain
- Manchado A., Stanghellini L., Guerrero M. A., 1996b, *ApJ*, 466, 95
- Meaburn J., López J. A., Gutiérrez L., Quirós F., Murillo J. M., Valdez J., Pedrayes M., 2003, *RevMexAA*, 39, 185
- Medina J. J., Guerrero M. A., Luridiana V., Miranda L. F., Riera A., Velázquez P. F., 2007, in Corradi R. L. M., Manchado A., Soker A., eds, *Asymmetrical Planetary Nebulae IV*, Proceedings in electronic book (<http://www.iac.es/proyecto/apn4/pages/proceedings.php>).
- Miranda L. F., Solf J., 1992, *A&A*, 260, 397
- Miranda L. F., Ayala S., Vázquez R., Guillén P. F., 2006, *A&A*, 456, 591
- Miranda L. F., Ramos-Larios G., Guerrero M. A., 2010, *PASA*, 27, 180
- Sabbadin F., 1984, *MNRAS*, 210, 341
- Sabin L., Vázquez R., López J. A., García-Díaz Ma. T., Ramos-Larios G., 2012, *RevMexAA*, 48, 165
- Sahai R., 2000, *ApJ*, 537, L43
- Sahai R., Nyman L.-A., Wotten A., 2000, *ApJ*, 543, 880
- Schneider S. E., Terzian Y., Purgathofer A., Perinotto M., 1983, *ApJ*, 52, 399
- Schwarz H. E., Corradi R. L. M., Melnick J., 1992, *A&ASS*, 96, 23
- Vaytet N. M. H. et al., 2009, *MNRAS*, 398, 385
- Vázquez R., Torrelles J. M., Rodríguez L. F., Gómez Y., López J. A., Miranda L. F., 1999, *ApJ*, 515, 633
- Vázquez R., Miranda L. F., Olguín L., Ayala S., Torrelles J. M., Contreras M. E., Guillén P. F., 2008, *A&A*, 481, 107
- Velázquez P. F., Raga A. C., Riera A., Steffen W., Esquivel A., Cantó J., Haro-Corzo S., 2012, *MNRAS*, 419, 3529
- Wang W., Liu X.-W., Zhang Y., Barlow, M. J., 2004, *A&A*, 427, 873